Origin of the Planar Hall Effect in Nanocrystalline $Co_{60}Fe_{20}B_{20}$

K. M. Seemann,[1,*] F. Freimuth,[2] H. Zhang,[2] S. Blügel,[2] Y. Mokrousov,[2] D. E. Bürgler,[1] and C. M. Schneider[1]

[1]*Peter Grünberg Institute (PGI-6) and Jülich-Aachen Research Alliance (JARA-FIT), Forschungszentrum Jülich, D-52425 Jülich, Germany*

[2]*Peter Grünberg Institute (PGI-1), Institute for Advanced Simulation, and Jülich-Aachen Research Alliance (JARA-FIT), Forschungszentrum Jülich, D-52425 Jülich, Germany*

(Received 26 October 2010; published 19 August 2011)

An angle dependent analysis of the planar Hall effect (PHE) in nanocrystalline single-domain $Co_{60}Fe_{20}B_{20}$ thin films is reported. In a combined experimental and theoretical study we show that the transverse resistivity of the PHE is entirely driven by anisotropic magnetoresistance (AMR). Our results for $Co_{60}Fe_{20}B_{20}$ obtained from first principles theory in conjunction with a Boltzmann transport model take into account the nanocrystallinity and the presence of 20 at. % boron. The *ab initio* AMR ratio of 0.12% agrees well with the experimental value of 0.22%. Furthermore, we experimentally demonstrate that the anomalous Hall effect contributes negligibly in the present case.

DOI: 10.1103/PhysRevLett.107.086603 PACS numbers: 72.25.Ba, 71.70.Ej, 72.15.Gd

Electron transport effects employing the electronic spin degree of freedom lie at the heart of spintronics and its applications not only in information technology [1] but more increasingly also in sensorics for biomedical purposes, where the utmost sensitivity for detecting minute magnetic stray fields is needed. The planar Hall effect (PHE) and the anomalous Hall effect (AHE) as well as tunneling magnetoresistance are promising phenomena for realizing highly sensitive sensors. From a materials point of view, nanocrystalline $Co_{60}Fe_{20}B_{20}$ (CoFeB) attracts growing attention since it combines large saturation magnetization with low coercivity [2,3], both favoring high sensitivities.

PHE and AHE are both observed as a voltage transverse to the applied current [4,5] in contrast to the anisotropic magnetoresistance (AMR), which is measured in the longitudinal geometry. For PHE the magnetization $\mathbf{M}$ lies in the plane spanned by the current density $\mathbf{j} = j\mathbf{e_x}$ and the direction $\mathbf{e_y}$ of the transverse voltage measurement, and for AHE the component of $\mathbf{M}$ perpendicular to $\mathbf{j}$ and $\mathbf{e_y}$ matters. Although AMR has been known since Thomson's—later known as Lord Kelvin—observations in 1856 [6], PHE was discovered only a century later in polycrystalline permalloy [7]. More recently, PHE has also been found in crystalline $La_{2/3}Fe_{1/3}MnO_3$ [8] and as a very large effect at low temperatures in the dilute magnetic semiconductor (Ga,Mn)As [9]. The transverse resistance ρ_{xy} characterizing the PHE and the longitudinal resistivity ρ_{xx} denoting the AMR are given by [10]

$$\rho_{xy} = (\rho_{\parallel} - \rho_{\perp}) \sin\Phi \cos\Phi$$
$$\rho_{xx} = \rho_{\perp}\left(1 + \frac{\rho_{\parallel} - \rho_{\perp}}{\rho_{\perp}} \cos^2\Phi\right), \quad (1)$$

where $\rho_{\parallel}$ ($\rho_{\perp}$) is the resistivity along (perpendicular to) the direction of the in-plane component of $\mathbf{M}$, and Φ is the angle enclosed by $\mathbf{j}$ and $\mathbf{M}$. A transverse voltage arises whenever the current is neither perpendicular nor parallel to the magnetization. Even though the AMR is a subtle spin-orbit effect, quantitatively reliable predictions from first principles based on the density functional theory (DFT) can be made [11,12].

In this Letter, we elucidate the role of AMR in the PHE in nanocrystalline $Co_{60}Fe_{20}B_{20}$ thin films experimentally and by *ab initio* calculations. We measure AMR and PHE in longitudinal and transverse four-probe transport experiments. The single-domain behavior enforced by an exchange bias underlayer enables a direct comparison with theory, and we calculate AMR and PHE signals by the semiclassical Boltzmann approach using electronic structure calculated from first principles. In order to account for the nanocrystallinity of our real CoFeB system, an angular averaging of the conductivity tensor is performed. More specifically, we first calculate $Co_{0.75}Fe_{0.25}$ (CoFe) without boron as the magnetically equistoichiometric pendant to $Co_{60}Fe_{20}B_{20}$ and employ the virtual crystal approximation (VCA) [13] to take the disorder of CoFe into account. In the case of CoFeB we use a combined supercell plus VCA approach. In view of the residual [110] texture that has been found for CoFeB films [14], a possible contribution to the transverse resistivity by anisotropic Berry-phase AHE is also examined [15]. However, in our measurements it is found to be negligible. Hence, we unambiguously show that PHE has the same physical origin as AMR by verification of the experimentally obtained transport data with a first principles approach.

Our experimental system consists of magnetron-sputtered CoFeB with nanocrystalline morphology. We deposit films of 20 nm thickness *in situ* at room temperature (RT) on an antiferromagnetic $Ir_{20}Mn_{80}$ underlayer. The exchange interaction between the antiferromagnet and the ferromagnet induces a unidirectional exchange

anisotropy with the exchange bias field $\mathbf{H}_{ex}$ oriented along $\mathbf{e}_y$—perpendicular to the long axis of the Hall bar. We measure the resistivities ρ_{xy} and ρ_{xx} in the typical Hall geometry with a Hall contact size of 25×25 μm^2 at RT by recording the transverse and longitudinal voltage signals, respectively. The external field $\mathbf{H}$ is applied in the film plane and swept between -70 and $+70$ mT, while the sample is rotated around the film normal against $\mathbf{H}$ in steps of 5°. The rotation angle Φ_H is measured with respect to $\mathbf{H}_{ex}$. The resistivity ρ_{xx} obtained is shown in Fig. 1(a) after subtraction of a constant offset and yields the AMR, which is accompanied by a transverse resistivity ρ_{xy}, the PHE, displayed in Fig. 1(b) after subtraction of a geometry-related offset.

In our experiments we control the direction Φ_H of the external field, which does not necessarily coincide with the direction of $\mathbf{M}$. In particular, at small magnetic fields and in the presence of magnetic anisotropy we have to introduce the angle β between $\mathbf{H}$ and $\mathbf{M}$, which can be derived analytically from the Stoner-Wohlfarth model based on coherent single-domain behavior. Minimizing the free-energy density $E = -MH\cos(\beta) - MH_{ex}\cos(\Phi_H - \beta)$ comprising Zeeman and exchange bias contributions, we obtain

$$\beta = \arctan\left(\frac{H_{ex}\sin\Phi_H}{H + H_{ex}\cos\Phi_H}\right). \quad (2)$$

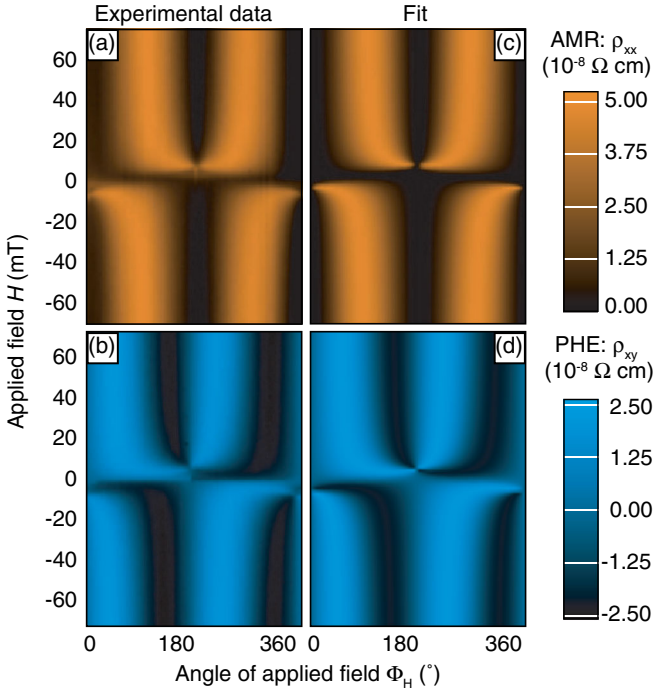

FIG. 1 (color online). Experimental resistivities ρ_{xx} (a) and ρ_{xy} (b) measured at RT as a function of field magnitude H and direction Φ_H. Corresponding fits using Eqs. (1) are shown in (c) and (d) and yield a RT AMR ratio of $(\Delta\rho/\rho)_{expt} = 0.22\%$.

In our case $\mathbf{H}_{ex}$ is perpendicular to $\mathbf{j}$ and we set in Eqs. (1) $\Phi = 90° + \beta - \Phi_H$ to obtain expressions that can be fitted to the experimental ρ_{xx} and ρ_{xy} data in order to determine the intrinsic AMR ratio $[(\rho_\parallel - \rho_\perp)/\rho_\perp]_{expt} \equiv (\Delta\rho/\rho)_{expt}$.

Least-squares fits of Eqs. (1) using Eq. (2) to the AMR and PHE data in Figs. 1(a) and 1(b) are displayed in Figs. 1(c) and 1(d). We find good agreement for all applied fields $\mathbf{H}$. Note that the total variations of both ρ_{xx} and ρ_{xy} amount to the same value 5.0×10^{-8} Ω cm as expected from Eqs. (1). Therefore, our data confirm the magnetic single-domain behavior of the CoFeB film. The fits consistently yield an exchange bias field $H_{ex} = 5.2$ mT and a RT AMR ratio of $(\Delta\rho/\rho)_{expt} = 0.22\%$.

We also observe a strong temperature dependence of the PHE signal, which we investigate in the temperature range between RT and 10 K for two pronounced field directions: For $\Phi_H = 45°$ we observe typical AMR hysteresis loops [Fig. 2(a)], and for $\Phi_H = 90°$ the curves assume the characteristic shape of hysteretic Hall loops [Fig. 2(b)]. The PHE curves for $\Phi_H = 45°$ are asymmetric and shifted by H^* on the field axis due to the exchange bias effect. The shift at RT of 1.7 mT is less than $H_{ex} = 5.2$ mT determined

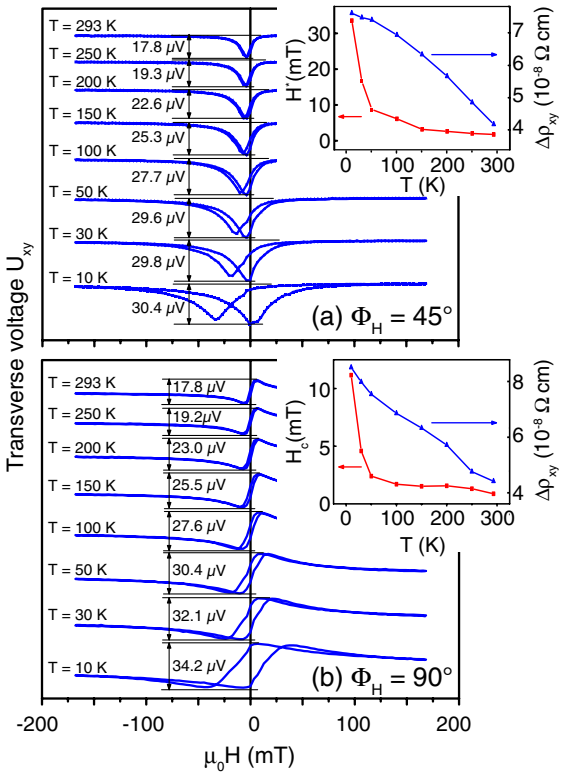

FIG. 2 (color online). Temperature dependence of the measured PHE signal U_{xy} for (a) $\Phi_H = 45°$ and (b) $\Phi_H = 90°$. The curves are vertically offset for clarity and the ΔU_{xy} values are given for each temperature. Insets: Evolution with temperature of the field shift H^* and coercivity H_c, respectively, together with the field-dependent amplitude $\Delta\rho_{xy}$ around zero field.

from the transport data in Fig. 1 since the field is applied at an angle with respect to $\mathbf{H}_{\mathrm{ex}}$. The curves for $\Phi_H = 90°$ represent hard-axis loops and are completely symmetric with respect to $H = 0$. The coercive field H_c of the hysteretic Hall loops evolves very similar to the exchange bias shift of the $\Phi_H = 45°$ data [lower (red) curves in the insets of Fig. 2]. The temperature dependence of the PHE signal variation around zero applied field $\Delta\rho_{xy}$ is also depicted in the insets of Fig. 2. Interestingly, the field shift H^* increases at lower temperatures, only making it more obvious that the PHE signal ρ_{xy} is actually a manifestation of the AMR. A further point of evidence for the AMR nature of ρ_{xy} is that the field-dependent amplitude $\Delta\rho_{xy}$ around zero field scales negatively with increasing temperature, unlike AHE does [5].

We performed DFT calculations of the electronic structure of CoFe and CoFeB using the full-potential linearized augmented plane wave (FLAPW) code FLEUR [16] and the generalized gradient approximation. For the theoretical description of disordered bcc CoFe we make use of the VCA [13]. Using a 6.8 hartree plane-wave cutoff and a $20 \times 20 \times 20$ k mesh, the computed theoretical lattice constant for $Co_{0.75}Fe_{0.25}$ is 0.282 nm and the average spin magnetic moment is $2.02\mu_B$, in very good agreement with calculations based on the coherent potential approximation [17]. Within the FLAPW method VCA is only applicable to binary alloys with both atomic species adjacent in the periodic table. Thus, we employ a combined supercell plus VCA approach for $Co_{60}Fe_{20}B_{20}$. Experimentally, it has been found that boron predominantly fills interstitial sites in bcc CoFeB alloys rather than substituting for transition metal sites, and that the bcc CoFe lattice does not expand upon addition of boron [18–20]. Hence, we set up a bcc supercell consisting of 4 VCA CoFe atoms into which we included one boron atom at an interstitial site. In units of the lattice constant specified above, the Cartesian coordinates of the VCA atoms are $(0, 0, 0)$, $(\frac{1}{2}, \frac{1}{2}, \frac{1}{4})$, $(0, 0, \frac{1}{2})$, $(\frac{1}{2}, \frac{1}{2}, \frac{3}{4})$. The boron atom is located at $(\frac{1}{4}, \frac{1}{2}, 0)$. Since an angular averaging of the resistivity tensor will be performed later, it is sufficient for the purposes of this study to take only this single configuration into account, instead of performing a configurational averaging. The calculated average spin magnetic moment per magnetic VCA atom of $1.27\mu_B$ is in good agreement with the value of $1.1\mu_B$, which we measure experimentally for $Co_{60}Fe_{20}B_{20}$.

In order to obtain the AMR ratio, $(\Delta\rho/\rho)_{\mathrm{theor}}$, from first principles, we compute the conductivity tensor σ, which within the Boltzmann theory is given by

$$\sigma = \frac{\tau e^2}{\hbar^2 V N} \sum_{\mathbf{k}n} (\nabla_{\mathbf{k}} \epsilon_{\mathbf{k}n}) \otimes (\nabla_{\mathbf{k}} \epsilon_{\mathbf{k}n}) \delta(\epsilon_{\mathbf{k}n} - \epsilon_F), \qquad (3)$$

with N as the number of k points and V as the unit-cell volume. τ denotes the relaxation time (which we assume to be $\mathbf{k}$ independent), $\epsilon_{\mathbf{k}n}$ is the single particle energy of band n at k point $\mathbf{k}$, and ϵ_F is the Fermi energy. The group velocity associated with the electron in band n is $\mathbf{v}_{\mathbf{k}n} = (1/\hbar)\nabla_{\mathbf{k}} \epsilon_{\mathbf{k}n}$. Spin-orbit interaction causes a dependence of the band energies $\epsilon_{\mathbf{k}n}$—and consequently also of the conductivity tensor σ—on the direction of the magnetization $\mathbf{M}$ leading to AMR. The δ function in Eq. (3) is approximated by a Gaussian of width $\frac{\pi}{(NV)^{1/3}} |\nabla_{\mathbf{k}n} \epsilon_{\mathbf{k}n}|$. In order to compute Eq. (3) computationally efficiently we use Wannier interpolation [21,22].

Equation (3) is evaluated for 26 different magnetization directions $\hat{\mathbf{M}} = (\sin\theta\cos\varphi, \sin\theta\sin\varphi, \cos\theta)$ in both CoFe and CoFeB. The resistivity tensor $\rho(\hat{\mathbf{M}}) = \sigma^{-1}(\hat{\mathbf{M}})$ is expanded in terms of the directional cosines of the magnetization [23]. We found that in order to fit our data it is sufficient to cut the expansion after the 4th order term. The longitudinal resistivity along the unit direction $\hat{\mathbf{e}}_\zeta$ ($\zeta = r, \theta, \varphi$) in spherical coordinates is given by the projection $\rho_\zeta(\hat{\mathbf{M}}) = \hat{\mathbf{e}}_\zeta \rho(\hat{\mathbf{M}}) \hat{\mathbf{e}}_\zeta$. The two resulting $\hat{\mathbf{M}}$-dependent AMR ratios are given by $[\rho_r(\hat{\mathbf{M}}) - \rho_\theta(\hat{\mathbf{M}})]/\rho_r(\hat{\mathbf{M}})$ and $[\rho_r(\hat{\mathbf{M}}) - \rho_\varphi(\hat{\mathbf{M}})]/\rho_r(\hat{\mathbf{M}})$. The angular dependence of the AMR ratios in ordered bcc CoFe displays cubic symmetry. In the case of the CoFeB supercell, the inclusion of boron violates the cubic symmetry and therefore the resistivity exhibits an additional geometrical anisotropy in addition to the anisotropy due to the spin-orbit interaction. However, this geometrical anisotropy may be eliminated easily by defining a new effective resistivity tensor, which is given by the sum of resistivity tensors rotated about the [111] direction. Consider, for example, the matrix elements $\rho_{xx}(\hat{\mathbf{e}}_x)$, $\rho_{yy}(\hat{\mathbf{e}}_y)$, and $\rho_{zz}(\hat{\mathbf{e}}_z)$. From these the matrix element $\bar{\rho}_{xx}(\hat{\mathbf{e}}_x) = [\rho_{xx}(\hat{\mathbf{e}}_x) + \rho_{yy}(\hat{\mathbf{e}}_y) + \rho_{zz}(\hat{\mathbf{e}}_z)]/3$ is constructed, and $\bar{\rho}_{yy}(\hat{\mathbf{e}}_y) = \bar{\rho}_{zz}(\hat{\mathbf{e}}_z) = \bar{\rho}_{xx}(\hat{\mathbf{e}}_x)$. The resistivities for the other matrix elements and general magnetization directions are obtained analogously.

The resulting AMR ratios of the effectively cubic CoFeB system are shown together with those of CoFe for $\theta = 90°$ and $\theta = 45°$ in Figs. 3(a) and 3(b), respectively. The angular dependence of the AMR ratios is rather strong, as expected for single crystals [24,25]. The main effect of adding boron is a reduction of the AMR ratios while qualitatively the angular dependence of the AMR ratios is similar in the CoFe and CoFeB systems. The strong angular dependence clearly shows that calculations for many magnetic configurations have to be performed in order to calculate the polycrystalline average reliably.

In order to describe a nanocrystalline material in the absence of texture we average over all possible grain orientations. Then the resistivities $\rho_\parallel$ and $\rho_\perp$ are related to the angular averages of the projected resistivities $\langle\rho_r(\hat{\mathbf{M}})\rangle$ and $\langle\rho_\theta(\hat{\mathbf{M}}) + \rho_\varphi(\hat{\mathbf{M}})\rangle/2$, respectively. This procedure yields for VCA in CoFe an AMR ratio of $(\Delta\rho/\rho)_{\mathrm{theor}} = 0.19\%$. For CoFeB a smaller AMR ratio of 0.12% is obtained, which is in good agreement with the experimentally determined value of $(\Delta\rho/\rho)_{\mathrm{expt}} = 0.22\%$ considering the approximations made.

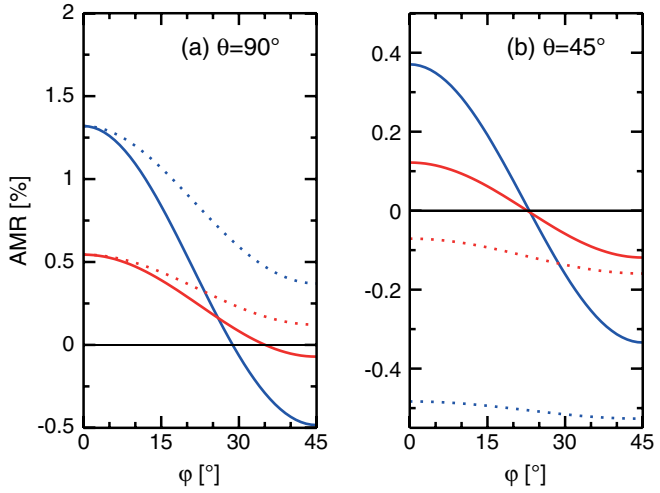

FIG. 3 (color online). Calculated $\hat{\mathbf{M}}$-dependent AMR ratios as a function of the azimuthal angle φ for (a) $\theta = 90°$ and (b) $\theta = 45°$. $Co_{75}Fe_{0.25}$ is illustrated in dark gray (blue) while $Co_{60}Fe_{20}B_{20}$ is light gray (red). The solid lines denote $(\rho_r - \rho_\varphi)/\rho_r$ and the dotted curves are $(\rho_r - \rho_\theta)/\rho_r$.

Since a residual [110] texture has been found in CoFeB films [14] that can give rise to a magnetization component perpendicular to the film, we also examine the possibility that the transverse signals shown in Figs. 1 and 2 may partly be governed by the anomalous Hall effect [26]. We have performed a computational assessment of the intrinsic AHE based on the topological Berry curvature of Bloch electrons in single-crystalline bcc $Co_{0.75}Fe_{0.25}$ and also in single-crystalline $Co_{60}Fe_{20}B_{20}$. We obtain—for the exaggerated case of a fully out-of-plane magnetized sample—anomalous Hall resistivities of $\rho^{\mathrm{AHE}}_{\mathrm{CoFe}} \approx 2.0 \times 10^{-7}\ \Omega\,\mathrm{cm}$ and $\rho^{\mathrm{AHE}}_{\mathrm{CoFeB}} \approx 3.0 \times 10^{-7}\ \Omega\,\mathrm{cm}$, which both are 1 order of magnitude larger than the measured PHE signal shown in Figs. 1 and 2. The anisotropy in the computed Berry-phase AHE, dominant over other impurity and disorder driven contributions to the AHE anisotropy [15], gives a field-dependent amplitude of $\Delta\rho^{\mathrm{AHE}}_{\mathrm{CoFe}} \approx 1.3 \times 10^{-8}\ \Omega\,\mathrm{cm}$. In a controlled experiment, we apply a saturating magnetic field normal to the film plane of the Hall bar device, finding that in the case of full saturation the measured AHE signal merely yields 1/10 of the PHE signal. This indicates that the role of finite disorder present in a CoFeB sample is to significantly suppress the intrinsic AHE, and, correspondingly, its anisotropy, precluding any significant contribution to the measured field-dependent PHE signal.

In conclusion, we have elucidated in a joint experimental and computational approach that PHE in CoFeB originates from AMR without contributions from AHE. Experimentally this is exhibited by an angle and temperature dependent investigation of the transverse and longitudinal signal. Using band structure calculations and semiclassical Boltzmann transport theory to calculate AMR, we obtain good agreement with the experimental AMR ratio of nanocrystalline CoFeB. The maximal AHE measured in CoFeB is significantly smaller than the anisotropy of the Berry-phase AHE calculated for CoFe.

K. M. S. thanks A. T. Hindmarch, C. H. Marrows, B. J. Hickey, and Ph. Mavropoulos for fruitful discussions. Y. M. acknowledges the HGF-YIG Programme VH-NG-513 for funding and the Jülich Supercomputing Centre for computational time.

*k.seemann@fz-juelich.de

[1] I. Zutic, J. Fabian, and S. D. Sarma, Rev. Mod. Phys. **76**, 323 (2004).
[2] S. Ikeda *et al.*, Nature Mater. **9**, 721 (2010).
[3] A. Weddemann *et al.*, New J. Phys. **11**, 113027 (2009).
[4] N. Nagaosa, J. Sinova, and S. Onoda, Rev. Mod. Phys. **82**, 1539 (2010).
[5] K. M. Seemann *et al.*, Phys. Rev. Lett. **104**, 076402 (2010).
[6] W. Thomson, Proc. R. Soc. London **8**, 546 (1856).
[7] K. L. Yau and J. T. H. Chang, J. Phys. F **1**, 38 (1971).
[8] J. Li *et al.*, J. Phys. Condens. Matter **22**, 146006 (2010).
[9] H. X. Tang *et al.*, Phys. Rev. Lett. **90**, 107201 (2003).
[10] D. A. Thompson, L. T. Romankiw, and A. F. Mayadas, IEEE Trans. Magn. **11**, 1039 (1975).
[11] J. Banhart and H. Ebert, Europhys. Lett. **32**, 517 (1995).
[12] S. Khmelevskyi *et al.*, Phys. Rev. B **68**, 012402 (2003).
[13] L. Bellaiche and D. Vanderbilt, Phys. Rev. B **61**, 7877 (2000).
[14] Y. T. Chen and C. C. Chang, J. Alloys Compd. **498**, 113 (2010).
[15] E. Roman, Y. Mokrousov, and I. Souza, Phys. Rev. Lett. **103**, 097203 (2009).
[16] See http://www.flapw.de.
[17] M. Ležaić, P. Mavropoulos, and S. Blügel, Appl. Phys. Lett. **90**, 082504 (2007).
[18] C. L. Platt, N. K. Minor, and T. J. Klemmer, IEEE Trans. Magn. **37**, 2302 (2001).
[19] A. Yang *et al.*, J. Appl. Phys. **103**, 07E736 (2008).
[20] A. K. Rumaiz *et al.*, Appl. Phys. Lett. **96**, 112502 (2010).
[21] J. R. Yates *et al.*, Phys. Rev. B **75**, 195121 (2007).
[22] F. Freimuth *et al.*, Phys. Rev. B **78**, 035120 (2008).
[23] T. R. McGuire and R. I. Potter, IEEE Trans. Magn. **11**, 1018 (1975).
[24] R. P. van Gorkom *et al.*, Phys. Rev. B **63**, 134432 (2001).
[25] Y. Gondo and Z. Funatogawa, J. Phys. Soc. Jpn. **7**, 41 (1952).
[26] M. Bowen *et al.*, Phys. Rev. B **71**, 172401 (2005).